Phase-field modeling on morphological landscape of isotactic polystyrene single crystals

Haijun Xu, Rushikesh Matkar, and Thein Kyu*
Department of Polymer Engineering, The University of Akron, Akron, Ohio 44325, USA
(Received 20 May 2004; revised manuscript received 1 March 2005; published 15 July 2005)

Spatio-temporal growth of isotactic polystyrene single crystals during isothermal crystallization has been investigated theoretically based on the phase field model by solving temporal evolution of a nonconserved phase order parameter coupled with a heat conduction equation. In the description of the total free energy, an asymmetric double-well local free energy density has been adopted to represent the metastable melt and the stable solid crystal. Unlike the small molecule systems, polymer crystallization rarely reaches thermodynamic equilibrium; most polymer crystals are kinetically stabilized in some metastable states. To capture various metastable polymer crystals, the phase field crystal order parameter at the solidification potential has been treated to be supercooling dependent such that it can assume an intermediate value between zero (melt) and unity (perfect crystal), reflecting imperfect polycrystalline nature of polymer crystals. Two-dimensional simulations exhibit various single crystal morphologies of isotactic polystyrene crystals such as faceted hexagonal patterns transforming to nonfaceted snowflakes with increasing supercooling. Of particular interest is that heat liberation from the crystallizing front influences the curvature of the crystal-melt interface, leading to directional growth of lamellar tips and side branches. The landscape of these morphological textures has been established as a function of anisotropy of surface energy and supercooling. With increasing supercooling and decreasing anisotropy, the hexagonal single crystal transforms to the dense lamellar branching morphology in conformity with the experimental findings.

DOI: 10.1103/PhysRevE.72.011804 PACS number(s): 61.41.+e, 81.10.−h

I. INTRODUCTION

Polymer crystallization has drawn immense attention for several decades because of a rich variety of crystalline morphology encompassing single crystals to hierarchical structures such as sheaflike textures and spherulites [1,2]. By virtue of the connectivity of polymeric chains, polymer crystallization hardly reaches thermodynamic equilibrium; therefore crystals thus formed are imperfect containing sizable defects. It has been generally known that polymer single crystals can be grown from dilute solutions, whereas spherulites develop from the melt. Recently, it becomes apparent that various single crystals can be formed from the melt state, producing various fascinating patterns including diamond, snowflakes, or faceted hexagonal shapes [3–5].

Lovinger and Cais [6] examined the single crystal growth from the melt of poly(trifluoroethylene) exhibiting lamellar branched morphology, which was explained in the context of the diffusion limited aggregation. Reiter and Sommer [7] observed the fingerlike branched patterns during crystallization of poly(ethylene oxide) which has been attributed to the diffusion process. Sakai and co-workers [8] found tip-splitting crystal growth in thin films of poly(ethylene terephthalate) that evolves to a crystal morphology, called terrace. Taguchi *et al.* [3] who investigated the crystal growth of isotactic polystyrene (ITPS) showed morphology variation with decreasing crystallization temperature. At high crystallization temperatures, a hexagonal single crystal of ITPS formed. However, the faceted hexagonal plate transforms to nonfaceted snowflakes, then to dense branching morphology (compact seaweed) with decreasing temperature of crystallization.

Intrigued by the Taguchi and co-worker's experimental observation [3], we have simulated the spatial-temporal growth of polymer single crystals based on the phase field model [9–13]. Compared to the traditional solidification theory involving free boundary problems [14], the phase field model treats the crystal-melt boundary to be smooth, albeit sharp, with a finite interface thickness. In general, the solid-liquid interface is an active free boundary from which latent heat is liberated during phase transformation. A scalar phase field, termed crystal order parameter, ψ is introduced that distinguishes the two distinct phases, i.e., zero in the melt and unity in the crystalline region, but the value of ψ varies smoothly at the interface [11]. There are several phase field models which have their own merits [9–17]. The advantage of these phase field approaches is that the regions of melt and solid crystals are treated the same without the requirement of explicitly tracking the position of the melt-crystal interface, i.e., it is given implicitly by a set of scalar and/or tensorial functions of time and space. Thus the phase field approaches provide a convenient means of calculating realistic interfacial structures of the small molecule systems [9–12], thereby avoiding difficult boundary integral or domain transformation methods encountered in the free boundary problems [14].

The stability solution of the single phase field equation yields a planar (square or rectangular in two dimensions) or a circular interface of the crystal. However, the phase field equation is usually coupled with another spatio-temporal evolution equation representing self-generated temperature, mechanical, or concentration fields. The energy balance equation is necessary to express the self-generated thermal field during isothermal quiescent crystallization, which can account for highly curved interfaces. Such heat equation,

*Corresponding author. Electronic address: tkyu@uakron.edu

also known as the heat conduction equation, incorporates the latent heat liberated at the growing front, which in turn drives the directional solidification, exhibiting a variety of interfacial morphologies such as seaweed, cellular and dendritic patterns. A structure with pronounced orientational order is called dendrite, and without apparent orientational order it is called seaweed. The dendritic shape is a symmetric needle crystal with a parabolic tip affected on its sides by a secondary branching. The seaweed morphology was originally introduced on the basis of experimental observations under the name of dense-branching morphology, which is characterized by repeating tip splitting at the interface front. The coupled phase field equations have been successfully applied to epitaxial growth of snowflakes and metal alloys [11,12]. Recently, a single phase field equation has been used to simulate faceted growth of the polymer single crystals [13].

We are intrigued by the phase field model of Kobayashi [11] who applied a phase field model based on the anisotropic Landau-type potential [15] with some free model parameters in accounting for the dendritic growth of snowflakes. The two-dimensional simulation revealed the evolution of dendritic structures growing into an undercooled melt. Although the Kobayashi potential [11] is seemingly adequate for the description of the dendritic growth of the small molecule system, the extension of it to high molecular weight polymers requires appropriate modification as polymer crystallization may not achieve thermodynamic equilibrium during solidification due to the long chain nature of macromolecules. To capture the imperfect morphology of semicrystalline polymer crystals, the various metastable states of polymer crystallization must be incorporated in the phase field model. That is to say, the simulation based on this modification must account for the development of less-ordered incomplete spherulitic structures to highly ordered faceted single crystals of polymers by simply varying crystallization temperature or supercooling. A convenient starting point is the deployment of asymmetric free energy double well of Harrowell and Oxtoby [16] or of Chan [17] who expressed the phase field parameter at the solidification potential to be a constant, but it is less than unity.

In this paper, we modified the Harrowell-Oxtoby solidification potential to be supercooling dependent such that various metastable states of polymer crystallization as well as the spatio-temporal development of imperfect semicrystalline morphologies may be explained. The advantage of the present modified phase field model for polymer crystallization is that the model parameters may be evaluated directly from the experimentally measurable material parameters. In addition, all model parameters are shown to be supercooling dependent; that is to say, any changes in crystallization temperatures can influence the crystalline morphology drastically. The present paper demonstrates theoretically the morphological landscape of ITPS covering faceted hexagonal, dendritelike snowflakes to seaweed-type lamellar branching morphology during isothermal crystallization. Of particular importance is that the emerged morphology depends not only on supercooling, but also on the anisotropy of crystal surface energies. These predicted morphologies have been discussed in relation to the reported experimental morphologies of ITPS [3].

II. THEORETICAL DESCRIPTION

In the phase field modeling for solidification of a pure substance, the total free energy of the system, $F(\psi)$ may be described in terms of a combination of a local free energy density, $f_{\text{local}}(\psi)$ and a nonlocal free energy density representing interface gradient, $f_{\text{grad}}(\psi)$ involving a nonconserved crystal order parameter (ψ) [9–13] as

$$F(\psi) = \int f_{\text{cryst}}(\psi) dV = \int [f_{\text{local}}(\psi) + f_{\text{grad}}(\psi)] dV. \quad (1)$$

The temporal evolution of the order parameter can be expressed in accordance with the standard Ginzburg-Landau approach [13–15] as

$$\frac{\partial \psi(r,t)}{\partial t} = -\Gamma \frac{\delta F(\psi)}{\delta \psi(r,t)}, \quad (2)$$

where $\psi(r,t)$ representing the crystal order parameter at time t and position r, may be defined as $\psi = l/l_z$ which is analogous to linear crystallinity. Γ is the rotational mobility which is inversely proportional to the drag force or melt viscosity.

The melting temperature of polymer crystals obtained at a given crystallization condition is always lower than that of the equilibrium melting point. It is therefore reasonable to consider various metastable states in polymer solidification that reveal various hierarchy morphologies such as imperfect spherulites to highly ordered single crystals. To account for the various metastable states of defective polymer crystals, local free energy density of Harrowell-Oxtoby [16] has been adopted in which the system possesses an asymmetric double well with respect to ψ and the solidification potential at ζ_0,

$$f_{\text{local}}(\psi, T) = W \int_0^{\psi} \psi(\psi - \zeta)(\psi - \zeta_0) d\psi$$
$$= W\left(\frac{\zeta\zeta_0}{2}\psi^2 - \frac{\zeta + \zeta_0}{3}\psi^3 + \frac{\psi^4}{4} \right), \quad (3)$$

where the unstable energy barrier is ζ. The order parameter at the stable solidification potential is taken as $\zeta_0 = T_m/T_m^0$, where T_m^0 is the equilibrium melting temperature, T_m is the melting temperature obtained at a specific crystallization temperature T and W is a dimensionless coefficient describing the height of energy barrier for nucleation. We have modified the crystal order parameter at the solidification potential well, ζ_0 to be equal to T_m/T_m^0 so that its value is unity only at true thermodynamic equilibrium which is rarely realized in polymer crystallization. Generally speaking, ζ_0 can assume some finite values less than unity in a manner dependent on the experimental melting temperature, T_m, representing various metastable potentials. It should be emphasized that the crystal morphology as well as the emerged crystallinity is strongly dependent on the crystallization temperature. For instance, faceted single crystals (e.g., hexagonal single crystal in ITPS) develop at a higher crystallization temperature, whereas dense lamellar branching morphology (or spherulites) are formed at lower crystallization temperatures or larger supercooling. The crystal morphology, the emerged crystallinity, and the melting temperature are there-

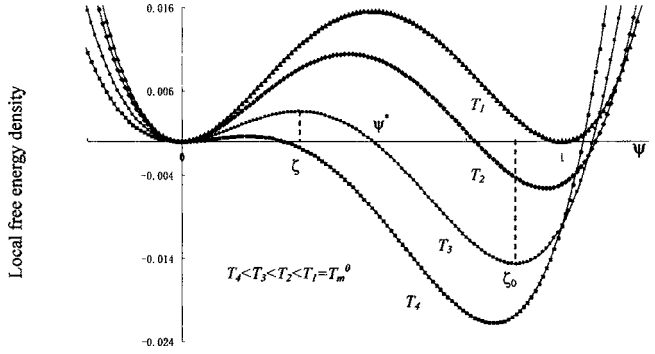

FIG. 1. Variation of the local free energy density as a function of crystal order parameter ψ for various temperatures showing different nucleation barrier heights and locations, ζ. The order parameter at the solidification potential, ζ_0, varies with the crystallization temperature as a result of the imperfection of polymer crystals.

fore strongly dependent on the crystallization temperature [18]. Undoubtedly, the local crystallinity of the single crystals would be higher than that of the spherulites due to the greater crystal perfection. However, since the population of single crystals obtained at higher crystallization temperatures is significantly smaller than those of the spherulites, the overall bulk crystallinity (or heat of fusion) of the sample containing single crystals could be smaller than that of spherulites in actual experiments [19]. The imperfect crystals tend to melt at a lower temperature relative to that of the crystals with a greater perfection. Undoubtedly, the dependence of the melting transition on crystalline morphology resulting from different crystallization conditions would be very complex. This is exactly why the aforementioned modification of the phase field crystal order parameter at the solidification potential, ψ_0 was needed to account for the imperfect nature of polymer crystals.

As demonstrated by Chan [15,17], if the coefficient of the third-power order parameter term of the Landau expansion were exactly zero, the local free energy displays two identical minima that differ only in sign which has been applied traditionally to the second order phase transition. To describe the first order phase transition such as polymer crystallization, it is imperative that the third order coefficient must be nonzero such that the double well is asymmetric with two minima with different energy levels in which $f(0)$ represents the melt, whereas $f(\zeta_0)$ signifies the metastable crystal with the nucleation barrier maximum at ζ (Fig. 1).

It should be emphasized that we have modified the crystal phase field order parameter representing the free energy well of the crystalline solid to depend on supercooling or crystallization temperature. As shown in Fig. 1, the order parameter at the potential well of the stable solid, ζ_0 can be varied from some finite values (imperfect crystals) to unity (perfect crystal), thereby capturing various metastable states of polymer solidification. At T_m^0 ($\zeta=0.5$), the two free energy densities have identical local minimum implying that the crystal and melt can coexist. When $T<T_m^0$ ($\zeta<0.5$), the free energy density has a global minimum at ψ_0 less than 1 representing the imperfect semicrystalline nature. Nonetheless, the solid state is more stable than the melt. Hence, the melt will undergo solidification by overcoming the nucleation barrier labeled by ζ on the ψ axis. As the supercooling (ΔT) increases, ζ_0 becomes significantly smaller than unity, which implies that the emerged crystal contains some crystal defects. The crystal thus formed is therefore imperfect, reflecting the complex morphology of semicrystalline polymers. It can be anticipated that the perfection of such metastable crystals could improve with increasing temperature of crystallization or annealing. The uniqueness of the proposed approach is that there is no need for taking into consideration the multiple metastable-wells in accounting for the multiple metastability potentials of polymer crystallization; a simple free energy double well with various (supercooling dependent) ζ_0 would serve the same purpose without losing any physical essence of the general solidification phenomena.

The nonlocal free energy density can be written in terms of the gradient free energy density describing the growth process as

$$f_{\text{grad}}(\psi) = \tfrac{1}{2}\kappa^2(\nabla\psi)^2, \tag{4}$$

where κ is the coefficient of interface gradient.

Substituting Eqs. (2)–(4) into Eq. (1), one obtains

$$\frac{\partial\psi(r,t)}{\partial t} = -\Gamma\frac{\delta F(\psi)}{\delta\psi} = -\Gamma(W\psi(\psi-\zeta)(\psi-\zeta_0) - \kappa^2\nabla^2\psi). \tag{5}$$

The first and the second terms signify the nucleation and interface growth processes, respectively. As will be demonstrated later, the interplay between these two competing processes eventually determines the final morphology of the emerging polymer crystal.

Another important factor in polymer crystallization is the self-generated temperature field created by the liberation of latent heat. In metallic alloys [20,21], heat conduction is very rapid such that the latent heat thus released may dissipate quickly. Hence, the temperature field may be treated as uniform. However, in most organic and polymeric materials, thermal conductivity is relatively slow, and therefore the liberated heat could exert appreciable effect on the crystal-melt interface, especially in the case of fast solidification. To determine the temperature distribution at the growing crystal fronts, a heat conduction equation may be deduced from the conservation law of enthalpy, i.e., the energy balance equation involving latent heat takes the form of

$$\rho C_p\frac{\partial T}{\partial t} = k_T\nabla^2 T + \rho\Delta H_u\frac{\partial\psi}{\partial t}, \tag{6}$$

where ρ (kg/m^3) is density, C_p (kJ/kg K) heat capacity, k_T (J/m s K) thermal conductivity, and ΔH_u (J/kg) latent heat. Let thermal diffusivity $\alpha=k_T/\rho C_p$ and $K=\Delta H_u/C_p$, then the heat conduction equation for the temperature evolution takes the form [11]

$$\frac{\partial T}{\partial t} = \alpha\nabla^2 T + K\frac{\partial\psi}{\partial t}. \tag{7}$$

In order to present the governing equations (6) and (7) in dimensionless form, the variables are rescaled to dimension-

less time τ and dimensionless variables denoted with tilde symbols as follows: $\tilde{x}=x/d^*$, $\tilde{y}=y/d^*$, $\tau=Dt/d^{*2}$, where the characteristic length for the single crystals d^* may be in the range of 10^{-8} (i.e., of the order of the lamellar thickness) to 10^{-7} m which is of the order of the radius of gyration of polystyrene chains [22], and the diffusion coefficient of ITPS is taken as $D=1\times10^{-9}$ m^2/s that gives $\Gamma=D/d^{*2}$ to be 10^5–10^7(s). This estimated value for ITPS is accidentally comparable to the value (10^5) determined by ^{13}C NMR of loose loops at the overlayer of polyethylene lamellar crystals [23]. The temperature is rescaled to $U=(T-T_x)/(T_m-T_x)$, where T_x is the experimental temperature of crystallization. Then, the final governing equations may be represented in dimensionless form (please see Appendix for detailed derivation),

$$\frac{\partial\psi(r,t)}{\partial\tau}=-\left\{W\psi(\psi-\zeta)(\psi-\psi_0)-\kappa_0^2\tilde{\nabla}[\beta^2(\Omega)\tilde{\nabla}\psi]+\kappa_0^2\left[\frac{\partial}{\partial\tilde{x}}\beta(\Omega)\beta'(\Omega)\right]\frac{\partial\psi}{\partial\tilde{y}}-\kappa_0^2\left[\frac{\partial}{\partial\tilde{y}}\beta(\Omega)\beta'(\Omega)\right]\frac{\partial\psi}{\partial\tilde{x}}\right\}, \tag{8}$$

where Ω is the orientation angle between the surface normal and the reference axis and the prime symbol denotes a derivative with respect to Ω, i.e., $d/d\Omega$. Similarly, Eq. (7) may be expressed in a dimensionless form as

$$\frac{\partial U}{\partial\tau}=\tilde{\alpha}\tilde{\nabla}^2U-\tilde{K}\frac{\partial\psi}{\partial\tau}, \tag{9}$$

where $\tilde{\nabla}=\tilde{i}(\partial/\partial\tilde{x})+\tilde{j}(\partial/\partial\tilde{y})$, $\tilde{\alpha}=\alpha/d^{*2}\Gamma$, $\kappa_0=\kappa/d^*$, and $\tilde{K}=\Delta H_u/C_pT_m$. ΔH_u is the heat of fusion of a perfect crystal [24,25]. However, in practice, when the crystallization temperature is lowered or the supercooling is increased, the orderness of the emerging structure is far from perfection, and thus its local degree of crystallinity would be lowered. Although ΔH_u of a pure substance is constant, its value for a polymer crystal would be strongly dependent on crystallinity, crystal morphology, and imperfection [24,25]. Since these morphological parameters depend on the crystallization temperature, i.e., K may be supercooling dependent through heat of fusion of polymer crystals, i.e., $K=\Delta H_u/C_p\propto\Delta T$. As cautioned by Kobayashi [11], this K should not be regarded as the true supercooling; K value should be estimated directly from the heat of fusion and heat capacitance whenever possible. However, it is often the case that these thermal quantities were not determined experimentally for each crystallization temperature, and thus ΔT may be taken as $(T_m^0-T_x)$ for the purpose of qualitative comparison. Moreover, T_m values may be estimated from T_x in accordance with the Hoffman-Week approach [24,3]. It should be emphasized that K remains constant during the course of isothermal crystallization at a given supercooling.

It should be emphasized that the Γ value, which is proportional to the rotational mobility, varies significantly from 10^{11} for metal alloys [16] to 10^2 for a polyethylene solid crystal [26], but it is of the order of 10^5 for amorphous loops

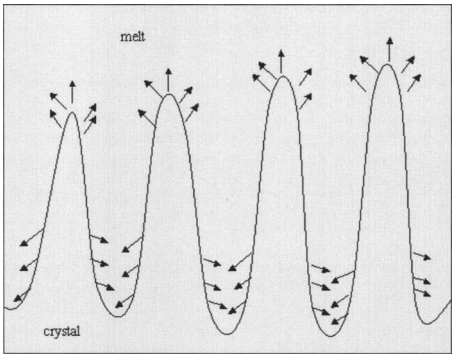

FIG. 2. A schematic drawing of the curved crystal-melt interface at which latent heat is generated nonuniformly in which the arrows indicate the approximate directions of heat flow from the highly curved interfaces. At the convex crystal-melt interface tips, the latent heat, thus generated, diffuses into the undercooled melt; whereas the heat is virtually accumulated at the concave regions.

at the lamellar surface of polyethylene crystals as evidenced by C^{13} NMR studies [23]. Now that all model parameters can be accessible through experimentally measurable quantities, except for the strength of anisotropy ε, the numerical calculation has been performed on the basis of Eqs. (A14) and (A15) in two dimensions on a square lattice using the finite central difference method for spatial discretization and the explicit forward method for time steps with a no-flux boundary condition. The crystal nucleation event was triggered with a single perturbation at the center of the grid to avoid overcrowding. Thermal noise was imparted at the interface such that the melt-solid interface retains some roughness by virtue of interface instability, i.e., $\eta=\eta_0\psi(1-\psi)$. This solid-melt interface also serves as a heat source as the heat is released through it. In the calculation, various grid sizes (128×128, 256×256, and 512×512) and temporal steps (Δt) have been employed to ascertain the stability of the simulation; however only the results of (512×512) calculation are shown.

III. RESULTS AND DISCUSSION

As depicted in Fig. 2, interfaces are generally rough having convex and concave curvatures. At convex tips, the heat may be dissipated readily into the melt and thus the crystal tip grows rapidly relative to that at the tail (or core). The exothermic latent heat generated during crystallization may be accumulated at concave regions where crystal growth is prohibited. This preferential heat conduction away from the convex solid-liquid tips and the heat entrapment in the case of concave curvature interface at the base has led to directional crystal growth. The nonuniform dissipation of heat at the irregular interface renders the growth of the interface to be complex, depicting a rich variety of morphological textures.

We are intrigued by the experimental observation of Taguchi and co-workers [3] who investigated the crystallization of ITPS single crystals in very thin films using atomic force microscopy (AFM) and transmission electron microscopy

TABLE I. Model parameters calculated from experimentally determined material parameters of ITPS at a given experimental temperature of 195 °C.

Material parameters	Model parameters
$\Delta H_u = 9.40 \times 10^4$ kJ/m^2 from Ref. [3]	$\Gamma = 10^5$ s^{-1}
$T_m^0 = 242$ °C from Ref. [3]	$W = 15.25$
$C_p = 1.80$ kJ/(kg K) from Ref. [24]	$\kappa_0^2 = 5.57 \times 10^{-12}$ m^2
$k_T = 0.128$ J/(m s K)	$\zeta = 0.18$
$\sigma_0 = 7.65 \times 10^{-4}$ kJ/m^2 from Ref. [3]	$\alpha = 6.58 \times 10^{-8}$ m^2/s
$\rho = 1080$ kg/m^3	$K = 48.4$ K
$\Gamma = 10^5$ s^{-1} from Ref. [23]	
$T_m = 229$ °C[a]	
$T_x = 195$ °C	

[a]Note that T_m may be estimated for each crystallization temperature T_x of 210 °C, 195 °C, and 180 °C from Ref. [3] and the model parameters thus calculated will vary accordingly.

(TEM). During crystallization of ITPS at 210 °C, these authors discovered that the emerged single crystal is a hexagon with the 110 growth facets [3,4]. With decreasing crystallization temperature, the 110 facets are no longer flat, and the interface structures change to curved hexagons, nonfaceted dendritelike snowflakes (at 195 °C), and then to seaweeds leading to dense lamellar branching morphology (at 180 °C). Furthermore, they concluded that the gradient of film thickness and the supercooling are responsible for the crystallization mechanisms changing from nucleation-dominated to diffusion-dominated growth that caused the unstable flat interface to undergo directional growth and eventually transforming to dendrites and seaweed-type dense branches.

These observed morphologies of ITPS single crystals present great challenge to us in testing the rigor of the present phase field theory of polymer crystallization. In our modified phase field approach, the model parameters were calculated in accordance with Eqs. (8), (9), and (A14)–(A18), using the experimentally accessible physical parameters for ITPS [3]. On the basis of the Week-Hoffman relationship [24], the equilibrium melting temperature of ITPS, T_m^0 was taken as 242 °C [3]. The experimental values of the materials parameters and experimental conditions, which were used in the determination of the model parameters, are tabulated in Table I. As demonstrated in the Appendix, all these model parameters are directly or indirectly related to supercooling. Hence, any variations in supercooling or crystallization temperatures could alter the model parameters that in turn could lead to the formation of rich variety of crystalline morphologies. At present, the relationship between anisotropy of the surface energy and supercooling is not known, thus the value of the anisotropy parameter is varied to determine its roles in the formation of interfacial morphology.

Figure 3(a) shows the simulated temporal-spatial growth of ITPS single crystal at an isothermal crystallization temperature $T = 210$ °C (corresponding to the supercooling of 32 K). With the anisotropy parameter, $\varepsilon = 0.09$, the growing single crystal resembles a hexagonal shape with faceted

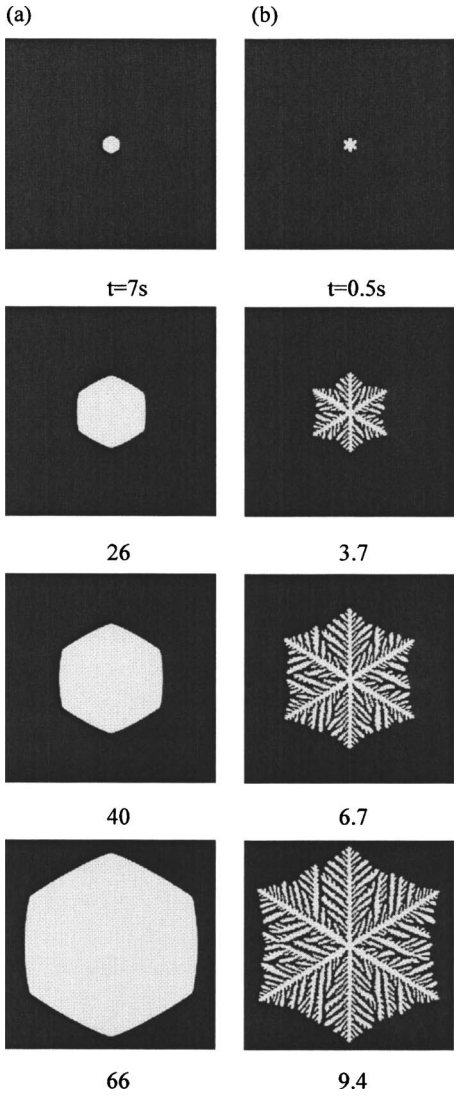

FIG. 3. The spatio-temporal growth of ITPS single crystal at crystallization temperatures of (a) 210 °C with $\varepsilon = 0.09$ and (b) 195 °C with $\varepsilon = 0.06$ in the crystal order parameter field calculated using the model parameters estimated from the material parameters some of which are listed in Table I, but under different experimental conditions. The simulation exhibits the spatio-temporal growth of (a) hexagonal plate with (110) facets and (b) dendritic growth. Note that the crystal-melt interface itself is the heat source, where the latent heat is liberated at any given instance.

(110) fronts. It is evident that at this shallow supercooling the crystal size remains unchanged until the entire edge has been filled, implying that the growth rate along the lateral edge (g) must be significantly greater than that normal to it (G). At the crystallization temperature of 195 °C and $\varepsilon = 0.06$, the growth rate was seemingly dominated by the diffusion as the supercooling gets deeper. The simulation at the supercooling of 47 K (i.e., at $T = 195$ °C) and anisotropy $\varepsilon = 0.06$ reveals the dendritic growth [Fig. 3(b)]. By virtue of the six-mode symmetry, the side lamellar branches have grown out at an approximate angle of 60° against the main lamellae.

The heat built-up can occur predominantly in the concave curvature regions where heat is seemingly entrapped. In such

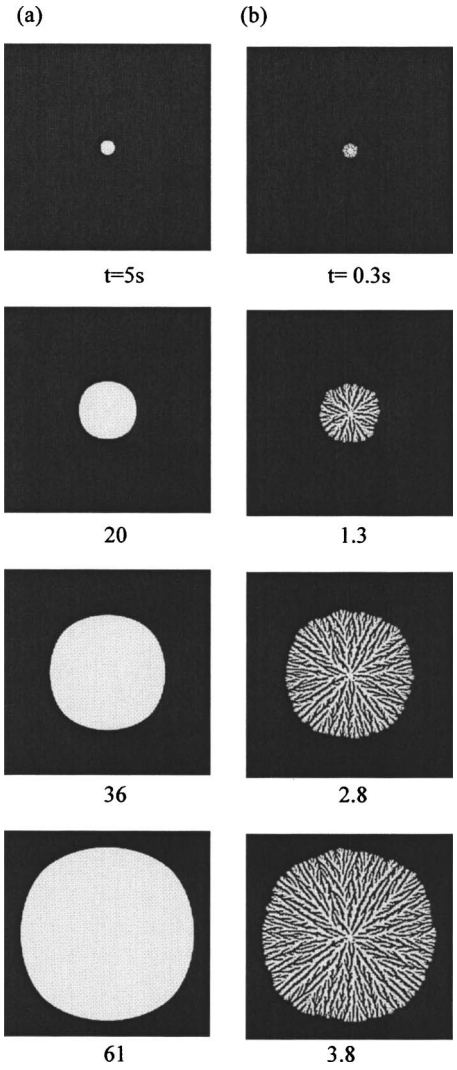

FIG. 4. The spatio-temporal isotropic growth of ITPS crystal at crystallization temperature (a) 210 °C with $\varepsilon=0$ and (b) 180 °C with $\varepsilon=0$ in the crystal order parameter field calculated using the material parameters some of which are listed in Table I but under different experimental conditions. The simulation exhibits the spatio-temporal growth of (a) spherical shape without internal structure and (b) lamellar branching morphology.

regions, crystallization is expected to be slow or in some cases ceased to continue in such concave regions due to the proximity of the advancing interfaces. It is evident that the heat dissipation may be faster at the convex tip than that at the concave interface, which permits the lamella to grow along the long lamellar axis. Concurrently, lamellar side-branching occurs by virtue of the rough edges of the growing lamellar sides. The nonuniform heat dissipation at the lamellar edges demarcates the interfacial boundaries of the crystal solid and the melt which is a manifestation of how the liberation of the latent heat can influence the polymer crystallization, particularly in the present ITPS.

In the absence of anisotropy, the simulations displayed the isotropic growth as depicted in Fig. 4. At the high crystallization temperature of 210 °C, the crystal is of the spherical shape without exhibiting any internal textures [Fig. 4(a)].

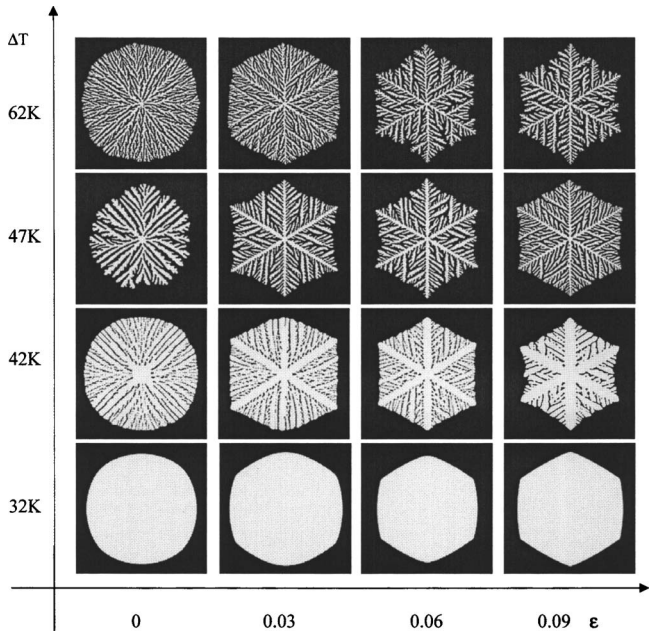

FIG. 5. Morphology diagram of ITPS as a function of supercooling and strength of surface energy anisotropy.

When the crystallization temperature is reduced to 180 °C, the main lamellae branch out from the sides and in some occasion, the main lamellar tip splits. Side-branching and tip-splitting (often called doublons) are common phenomena in the directional crystal growth in small molecule systems; hence polymer crystals are not exceptional to such occurrences. A continual creation and elimination of doublons are the typical characteristics of the seaweed growth. The lamellar side branching may be attributed to the directional growth of the lamellar crystals in which the heat release along the growing front is nonuniform due to the rough curvatures of the lamellar interface. That is to say the heat can dissipate readily from the convex lamellar tip, while the heat builds up at the concave core (see Fig. 2). The cascading side-branching continues from the existing side branches that eventually evolve into the dense lamellar branching morphology [Fig. 4(b)].

In addition to supercooling, the anisotropic properties of the solid-liquid interface play a particularly important role in determining the stability of the dendrites as well as the transformation between seaweed and dendrite morphology [11,20,21]. To describe the role of anisotropic surface energy in polymer crystallization, the coefficient κ is allowed to depend on the crystallographic orientation θ in accordance with Eqs. (A14) and (A17). This approach has been demonstrated by Kobayashi [11], as well as by McFadden and Wheeler [20,21] for small molecule systems such as dendritic growth in snowflakes and metal alloys.

A morphological diagram of ITPS has been established as a function of supercooling and anisotropy in Fig. 5, which discriminates among different interfacial patterns. At very low supercooling and high anisotropy, the faceted hexagonal pattern emerges. With increasing supercooling, the edges of the hexagon cave in, while the interface structure gradually transforms from hexagonal into nonfaceted dendrites. In the

absence of anisotropy at small supercooling, a circular pattern develops. With decreasing anisotropy at the shallow supercooling, the morphology transformation occurs from the hexagonal single crystal to the circular pattern through intermediate textures such as bulged (convex) hexagons. With increasing supercooling slightly, the hexagonal single crystals develop with curved edges, e.g., the curvature changes from circular to concave shape at the intermediate values of anisotropy. Upon further increasing supercooling, the edges of the hexagon split and form irregular branches, which may be characterized as degenerate and/or seaweed structure that eventually evolves to the dense lamellar branching morphology. It should be emphasized that not only the shape of crystal morphologies changes with supercooling, the length scale of the crystal changes, i.e., the mean width of branches and the average distance between neighboring lamellar branches decrease with increasing supercooling.

In the comparison between our simulated patterns and the experimental morphologies of the ITPS of Taguchi *et al.* [3], the faceted hexagonal single crystal changes to dendritic snowflakes and nonfaceted lamellar branching morphology in accordance with the combination of increasing supercooling and decreasing anisotropy of the interfacial energy. Usually the anisotropy parameter is difficult to measure experimentally; in many cases it is unknown. In this particular case, it gave us some clue that the anisotropy of the interfacial energy must be supercooling dependent as the anisotropy decreases as the supercooling increases. We must admit that the experimental single crystal structures of ITPS were obtained by first cooling the samples below the glass transition and then crystallizing them at some elevated temperatures. Hence, it is somewhat different from the direct temperature quench to the isothermal crystallization temperatures performed in our simulation, although the supercooling appears the same. Moreover, the importance of the thinness of the films on the emerging morphology has been emphasized by these authors [3], which has not been taken into account for our calculation. The sectorization was seen experimentally in the hexagonal single crystal of ITPS. However, we did not attempt to generate such sectorized hexagons here as an additional time-evolution equation pertaining to the chain tilting driven by the self-generated mechanical field is necessary. The feasibility of the sectorization based on the aforementioned approach has been already demonstrated by us for the syndiotactic and isotactic propylene single crystals [27,28], and therefore it is not repeated here. Nonetheless, the striking similarity between our simulated patterns and the experimentally observed morphologies [3] of ITPS certainly attests to the rigor of the phase field modeling.

IV. CONCLUSIONS

We have demonstrated that our modified phase field model is capable of accounting for the various metastable states of polymeric solids leading to spatio-temporal evolution of single crystals to hierarchical morphology driven by the self-generated thermal field. The crystal phase field order parameter at the solidification potential of the solid polymer crystal can be varied by simply changing supercooling anywhere between the threshold value to unity. Moreover, the model parameters can be estimated from the experimentally accessible physical parameters of ITPS. The two-dimensional simulation captured the resulting morphology varying from dense branch morphology to highly ordered faceted hexagonal single crystals, which are strikingly similar to the experimental results of Taguchi and co-workers [3]. The effects of anisotropy of surface energy and supercooling on the morphological landscape of ITPS have been demonstrated. With increasing supercooling and decreasing anisotropy, the lateral surface of ITPS crystals becomes unstable and undergoes morphological transition from the hexagonal plate to dendritelike snowflakes, and then to dense lamellar branching morphology. The resulting free energy expression thus accounts for metastability involving the latent heat generated at the crystal growth fronts.

ACKNOWLEDGMENTS

Support of this work by NSF Grant No. DMR 02-09272, CRDF Grant No. RC2-2398-02, and Ohio Board of Regent Research Challenge Grant is gratefully acknowledged. The authors are indebted to Dr. Leonid Manevitch and Dr. Elina Zubova, Semonov Institute of Chemical Physics, Russian Academy of Sciences, Moscow, for the fruitful discussion and constructive suggestions.

APPENDIX: NONDIMENSIONAL RENORMALIZATION FOR COMPUTATION

In order to make a valid comparison between the computations and the experiments, the model parameters, Γ, W, ζ, and κ, can be related to the real material parameters and the experimental conditions [29]. At a given crystallization temperature T, the crystal with an optimum lamellar thickness, l_z is formed due to a change in the free energy

$$\Delta f_{\text{local}} = 2A\sigma_e - Al_z\Delta H_u(1 - T/T_m^0), \tag{A1}$$

where σ_e is the surface free energy per unit area of the folded surface, A. Note that the surface energy of the lateral front is ignored. The crystal order parameter can be defined as $\psi = l/l_z$. In Fig. 1, it can be realized that at $\Delta f_{\text{local}}=0$, there existed a lamellar thickness $l^* < l_z$ beyond which the emerging crystal stabilizes. The threshold value, hereafter called stability order parameter, may be given as $\psi^* = l^*/l_z$, and thus

$$2\frac{\sigma_e}{l^*} - \Delta H_u(1 - T/T_m^0) = 0. \tag{A2}$$

According to the Hoffman and Weeks relationship [24,25], the melting temperature T_m of the crystal solidified at a given crystallization temperature T can be related to the lamellar thickness l_z,

$$2\frac{\sigma_e}{l_z} - \Delta H_u(1 - T_m/T_m^0) = 0. \tag{A3}$$

Then the stability order parameter could be determined from Eqs. (A2) and (A3) as described below [27],

$$\psi^* = \frac{l^*}{l_z} = \frac{T_m^0 - T_m}{T_m^0 - T}. \tag{A4}$$

Upon inserting Eq. (A4) into Eq. (3), the free energy barrier peak of crystallization, ζ can be expressed in terms of ψ^* and ζ_0, which are supercooling dependent,

$$\zeta = \frac{4\zeta_0\psi^* - 3\psi^{*2}}{6\zeta_0 - 4\psi^*}. \tag{A5}$$

On the other hand, from Eq. (3) the change in the local free energy density at the crystallization temperature T is expressed as

$$\Delta f_{\text{local}}^{\psi} = f_{\text{local}}(\psi_0) - f_{\text{local}}(0) = W\left(\frac{\zeta\zeta_0^3}{6} - \frac{\zeta_0^4}{12}\right). \tag{A6}$$

By equating the free energy densities of crystallization given by Eqs. (A1) and (A6), we obtain

$$2\frac{\sigma_e}{l_z nRT} - \frac{\Delta H_u}{nRT}(1 - T/T_m^0) = W\left(\frac{\zeta\zeta_0^3}{6} - \frac{\zeta_0^4}{12}\right).$$

Utilizing Eq. (A3), the parameter W can be expressed as

$$W = 6\frac{\Delta H_u}{nRT\zeta_0^3}\left(\frac{T_m - T}{T_m^0}\right)\left(\frac{\zeta_0}{2} - \zeta\right)^{-1}. \tag{A7}$$

According to Allen and Cahn's approach [23], the excess free energy per unit area in the interface region over the bulk phase is given as $\sigma/nRT = \int_0^1 \sqrt{2f^{\psi}}d\psi$. At $T = T_m$ we have

$$\frac{\sigma}{nRT} = \frac{\kappa}{6}\sqrt{\frac{W}{2}}, \tag{A8}$$

therefore

$$\kappa = 6\frac{\sigma}{nRT}\left(\frac{2}{W}\right)^{1/2}. \tag{A9}$$

Let us consider Eq. (5) in one dimension with a moving frame of reference under a uniform velocity of $v = \partial\psi/\partial t$; Eq. (5) can be transformed as

$$\kappa^2\frac{d^2\psi}{dx^2} + \frac{v}{\Gamma}\frac{d\psi}{dx} - \frac{\partial f}{\partial\psi} = 0. \tag{A10}$$

We seek a solution of the form $\psi = \psi(z)$, where $z = x - vt$ under the boundary condition of $\psi \to \zeta_0$ as $x \to -\infty$ and $\psi \to 0$ as $x \to +\infty$ [16], one finds a stationary solution

$$\psi(z) = \frac{\zeta_0}{\left[1 + \exp\left(z\zeta_0\sqrt{\frac{W}{2\kappa^2}}\right)\right]} \tag{A11}$$

with the selected velocity being

$$v = -\Gamma\kappa\left(\zeta - \frac{\zeta_0}{2}\right)\sqrt{W}. \tag{A12}$$

Note that this selected velocity does not necessarily represent the growth rate of polymer spherulites. Combining Eqs. (16) and (19), one obtains

$$\Gamma = \frac{\sqrt{2}}{12}v\left[\frac{\sigma}{nRT}\left(\frac{\zeta_0}{2} - \zeta\right)\right]^{-1}. \tag{A13}$$

As demonstrated by Kessler *et al.* [30], the surface energy σ is anisotropic and takes the form

$$\sigma(\Omega) = \sigma_0\beta(\Omega) = \sigma_0(1 + \varepsilon\cos j\Omega), \tag{A14}$$

where σ_0 is the reference surface energy which may be taken as σ_e for polymer single crystals, and ε is the strength of anisotropy. The orientation angle Ω is defined as the angle between the interface normal and the reference axis and j specifies the number of mode. For a hexagonal shape crystal such as snowflakes, $j = 6$. In the phase field modeling, the orientation angle is determined in terms of ψ using a normal vector to the interface, n, defined as

$$\bar{n} = \frac{\nabla\psi}{|\nabla\psi|} = \cos\Omega\hat{x} + \sin\Omega\hat{y} \tag{A15}$$

in which the orientation angle, Ω is taken as

$$\tan\Omega = \frac{\partial\psi/\partial y}{\partial\psi/\partial x}. \tag{A16}$$

The resulting gradient coefficient κ is expressed in relation to the anisotropy parameter as

$$\kappa = \kappa_0\beta(\Omega) = 6\frac{\sigma_0}{nRT}\left(\frac{2}{W}\right)^{1/2}(1 + \varepsilon\cos j\Omega). \tag{A17}$$

Thus, the modified time-evolution equation (5) after including the anisotropy may be described as

$$\begin{aligned}\frac{\partial\psi(r,t)}{\partial t} = -\Gamma\Bigg(& W\psi(\psi - \zeta)(\psi - \zeta_0) - \kappa_0^2\nabla\cdot(\beta^2(\Omega)\nabla\psi) \\ &+ \kappa_0^2\left(\frac{\partial}{\partial x}\beta(\Omega)\beta'(\Omega)\right)\frac{\partial\psi}{\partial y} \\ &- \kappa_0^2\left(\frac{\partial}{\partial y}\beta(\Omega)\beta'(\Omega)\right)\frac{\partial\psi}{\partial x}\Bigg),\end{aligned} \tag{A18}$$

where the prime symbol denotes a derivative with respect to Ω, i.e., $d/d\Omega$.

[1] P. H. Geil, *Polymer Single Crystals* (Krieger, Huntington, NY, 1973).
[2] B. C. Bassett, *Principles of Polymer Morphology* (Cambridge University Press, Cambridge, 1981).
[3] K. Taguchi, H. Miyaji, K. Izumi, A. Hoshino, Y. Miyamoto, and R. Kokawa, Polymer **42**, 7443 (2001).
[4] K. Taguchi, Y. Miyamoto, H. Miyaji, and K. Izumi, Macromolecules **36**, 5208 (2003).
[5] M. Wang, H. Braun, and E. Meyer, Polymer **44**, 5015 (2003).
[6] A. J. Lovinger and R. E. Cais, Macromolecules **17**, 1939 (1984).
[7] G. Reiter and J. U. Sommer, Phys. Rev. Lett. **80**, 3771 (1998).
[8] Y. Sakai, M. Imai, K. Kaji, and M. Tsuji, J. Cryst. Growth **203**, 244 (1999).
[9] G. Caginalp and P. C. Fife, Phys. Rev. B **33**, 7792 (1986).
[10] G. Caginalp and E. A. Sokolovsky, Appl. Math. Lett. **2**, 117 (1989).
[11] R. Kobayashi, Physica D **63**, 410 (1993).
[12] A. A. Wheeler, W. J. Boettinger, and G. B. McFadden, Phys. Rev. A **45**, 7424 (1992).
[13] T. Kyu, R. Mehta, and H.-W. Chiu, Phys. Rev. E **61**, 4161 (2000).
[14] E. Brener, H. Müller-Krumbhaar, D. Temkin, and T. Abel, Physica A **249**, 73 (1998).
[15] L. D. Landau, J. Exp. Theor. Phys. **7**, 19 (1937); **7**, 637 (1937).
[16] P. R. Harrowell and D. W. Oxtoby, J. Chem. Phys. **86**, 2932 (1987).
[17] S.-K. Chan, J. Chem. Phys. **67**, 5755 (1977).
[18] J. M. Schultz, *Polymer Materials Science* (Prentice Hall, New York, 1974), p. 187; A. S. Kenyon, R. C. Gross, and A. L. Wurstner, J. Polym. Sci. **40**, 159 (1959).
[19] H. Xu and P. Cebe, Macromolecules **38**, 770 (2005).
[20] A. A. Wheeler, B. T. Murray, and R. J. Schaefer, Physica D **66**, 243 (1993).
[21] G. B. McFadden, A. A. Wheeler, R. J. Braun, S. R. Coriell, and R. F. Sekerka, Phys. Rev. E **48**, 2016 (1993).
[22] S.-T. Sung, I. Nishio, G. Swislow, and T. Tanaka, J. Chem. Phys. **73**, 5971 (1980).
[23] K. Kuwabara, H. Kaji, M. Tsuji, and F. Horii, Macromolecules **33**, 7093 (2000).
[24] J. D. Hoffman and J. J. Weeks, J. Res. Natl. Bur. Stand., Sect. A **66A**, 13 (1962).
[25] J. D. Hoffman and J. I. Lauritzen, Jr., J. Res. Natl. Bur. Stand., Sect. A **65A**, 297 (1961).
[26] W.-G. Hu, C. Boeffel, and K. Schmidt-Rohr, Macromolecules **32**, 1611 (1999).
[27] R. Mehta, W. Keawwattana, and T. Kyu, J. Chem. Phys. **120**, 4024 (2004).
[28] R. Mehta, W. Keawwattana, A. L. Guenthner, and T. Kyu, Phys. Rev. E **69**, 061802 (2004).
[29] S. Allen and J. W. Cahn, Acta Metall. **27**, 1085 (1979).
[30] D. A. Kessler, J. Koplik, and H. Levine, Adv. Phys. **37**, 255 (1988).